PROCEEDINGS, 43rd Workshop on Geothermal Reservoir Engineering
Stanford University, Stanford, California, February 12-14, 2018
SGP-TR-213

# Imaging Shallow Outflow Alteration to Locate Productive Faults in Ormat's Brady's and Desert Peak Fields Using CSAMT

Matthew Folsom, Janice Lopeman, Doug Perkin, Matthew Sophy

Ormat Technologies Inc. 6225 Neil Road, Reno NV, 89511

mfolsom@ormat.com

Keywords: Geothermal, magnetotellurics, gravity, Brady's, Desert Peak, outflow, alteration.

## ABSTRACT

This paper details the results and interpretations from a 2017 CSAMT (controlled-source audio-magnetotelluric) survey collected at Ormat's Brady's and Desert Peak geothermal fields. The goals of the survey were to 1) image low-resistivity smectite-clay alteration caused by outflow of thermal fluids discharging along structures, 2) correlate alteration with structures using geologic mapping, subsurface data, and gravity/magnetic geophysical surveys, 3) integrate these structures into a geological model with the goal of optimizing the existing wellfield configuration. The CSAMT survey consisted of seven lines using 50m receiver dipoles and five lines using 100m dipoles for a total of 50km of survey line. Two transmitter locations were used during the survey, with survey lines spaced an average of 1km apart. Ormat's geophysicists processed the data using 1D and 2D inversions to investigate the resistivity distribution over the survey area. In both geothermal fields, the CSAMT survey identifies low-resistivity anomalies primarily confined to the Truckee River Formation. Depth-slices through the model domain show how alteration occurs at the shallowest depths near productive faults, and moves basin-ward once entrained in shallower flow paths. High concentrations of ions found in Desert Peak geothermal fluids make the distinction of smectite-clay alteration less clear along the outflow path.

## 1. INTRODUCTION

Low resistivity zones that cap convective geothermal systems have long been popular exploration targets. These zones, caused by the argillic alteration of host rocks to smectite-group clays, occur largely between 70 and 200°C (Ussher et al., 2000). Above this layer, alteration to zeolites produce more resistive features. At higher temperatures below the smectite zone, mixed-layer clays and chlorite alteration are also more resistive (Hulen and Lutz, 1999). Although these patterns are common in volcanic geothermal systems, a similar clay geometry is often associated with forced convection systems like those found in the Basin and Range Province of the western United States and in Turkey. A conceptual model of these systems can be found in Cumming (2009). In convective volcanic systems, the pattern of argillic alteration is often dome-shaped, and the altered zone acts as a natural seal on the system with very low permeability. An excellent example can be seen at Medicine Lake Volcano KGRA in northeastern California (Hulen and Lutz, 1999; Cumming and Mackie, 2010). In amagmatic systems, however, geothermal fluids rise along permeable zones as part of a deep regional flow system, aided by thermal buoyancy. When fluid is discharged near the surface, it cools and becomes entrained within shallower flow paths, moving down the hydrologic head gradient towards basins or other drainages. For some distance along this path, alteration to smectite and mixed-layer clays is still possible.

Mapping outflow alteration is made easier using resistivity geophysical techniques. Operating under the assumption that fluids discharge near the surface and then flow down-gradient, one exploration strategy is to map high-resolution resistivity data and follow it 'uphill' to its point of termination. This paper tests this theory using the results of a high-resolution CSAMT survey over two well-known geothermal systems – The Brady's and Desert Peak systems located in the Hot Springs Mountains in northwestern Nevada. The two systems represent different end-members in the Basin and Range province. The Brady's system lies along a 4km long, NNE normal fault zone marked by hot ground, mud pots, fumaroles and formerly by hot springs and geysers. The Desert Peak system, on the other hand, is a classic blind resource with no surface manifestation beyond a small area of mapped silicified sands (Faulds et al., 2010). It was the first blind system to be discovered in the southwestern U.S. (Benoit et al., 1982). We corroborate our findings with an improved gravity dataset and modeling efforts, to better identify fault structures in the area of interest.

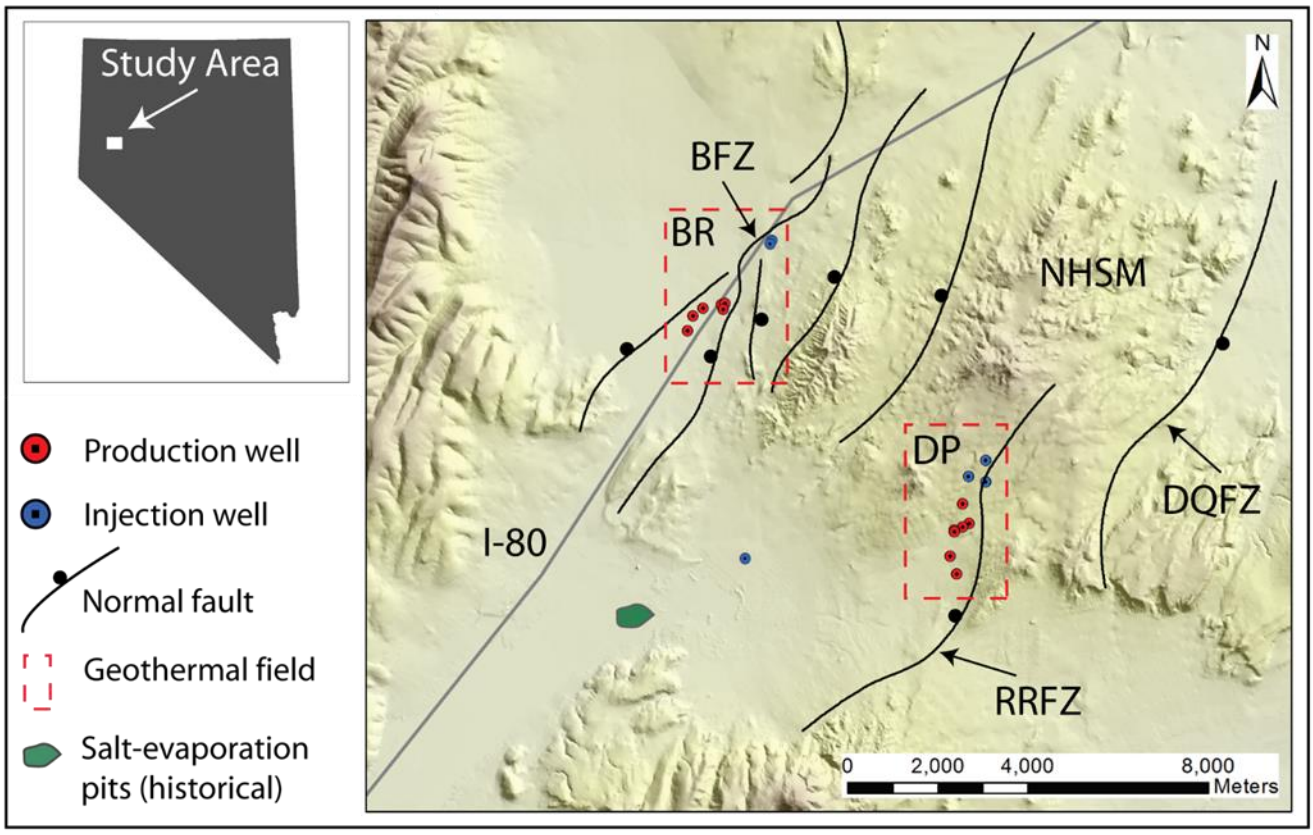


**Figure 1: Digital elevation model of the northern Hot Spring Mountains (NHSM) showing major faults zones and geothermal production areas. Faults are inferred from an updated gravity dataset (see Figure 2). Ball on fault lines denote the downthrown block. BFZ, Brady's fault zone; RRFZ, Rhyolite Ridge fault zone, DQFZ, Desert Queen fault zone; BR, Brady's geothermal field; DP, Desert Peak geothermal field.**

## 2. GEOLOGY

The northern Hot Springs Mountains are composed of thick sequences Oligocene to Pliocene volcanic rocks. These volcanic units have been divided into the lower Chlorapagus Formation and the upper Desert Peak Formation. This volcanic pile is in excess of 2km thick and overlies a sequence of Tertiary rhyolites and rhyodacites, henceforth referred to as the Rhyolite Formation. The basement, encountered by several wells in both Brady's and Desert Peak, is composed of Mesozoic metavolcanics and metasediments. In the Desert Peak region these units have been intruded in places by Cretaceous granodiorites (Benoit et al., 1982; Lutz et al., 2004). On top of the young volcanics are late Miocene to Pliocene sedimentary sequences of fresh water limestone, sandstone, diatomite and tuffaceous siltstones. These units are often interlaced with volcanic rocks and are collectively referred to as the Truckee River Formation. Pliocene and younger tufa is common, and evidence of prehistoric lake Lahonton shorelines is found along basin margins. The region is dominated by multiple sets of parallel, NNE trending, steeply dipping normal faults. Normal faulting in the field dips both WNW and to the ESE. This faulting has cut the Hot Springs Mountains into tilted, NNE trending fault blocks (Benoit et al., 1982; Faulds et al., 2003). Structural data and recent geochronology work suggests that a major pulse of extension occurred between 13 and 9 Ma, but continued in more recent times (Faulds et al., 2006).

The Brady's geothermal system is located along the Brady's Fault Zone (BFZ), a steeply dipping (~67°) network of at least three, closely-spaced (~1km) normal faults that separate the Hot Springs Flat Basin to the NW from the Hot Springs Mountains to the SE. Some production wells pull fluids from beneath the Truckee River Formation at fault intersections between 1100 and 1800ft deep. A second set of deeper production wells, west of I-80, source fluids from the fractured Rhyolite Formation between 2800 and 5900ft deep. Injection occurs north of the producing field and into shallower depths of the BFZ (< 1000ft). In more recent years, injection was added to the south and in a separate basin, believed to be somewhat less connected to the main field. This change in the injection program followed from short transient times between injecting and producing wells that impacted operations. At least one east-dipping normal fault immediately east of the BFZ, seen most prominently in gravity data, suggest that the BFZ bounds a small horst on its western side. Some workers have speculated that high fluid transmissivity at Brady's is enhanced by a small left step-over in the fault (Faulds et al., 2006; 2010).

The Desert Peak blind geothermal system sets upon the Rhyolite Ridge fault zone (RRFZ), a normal fault that accommodates structural offset on the order of 1000ft (Benoit, 1995). South of the Desert Peak wells the RRFZ is a noticeable feature, easy to see in satellite imagery and bounding a small basin to the east. Near the wells, however, the fault is subdued in both topography and geologic offset.

The fault zone here is believed to be concealed by forced folds, where basement-piercing faults do not break the surface, but bend the upper strata (Benoit, 1995). This structure may also contribute to why Desert Peak is a blind system. The productive portion of the field is located at a major step-over and relay ramp in the RRFZ, with numerous fault strands between the steps (Faulds et al., 2010). The gravity anomaly in this area is subdued and rather flat (Figure 2A), but the first vertical derivative of the anomaly suggest it is a prominent feature (Figure 2 B). Another possible explanation for the subdued gravity anomaly is that younger, dense volcanic flows may have filled paleo-valleys along hanging wall side of some faults (Lutz et al., 2009). Desert Peak wells produce mostly from fractured intervals in the Rhyolite Formation and the pre-tertiary basement. Performance of the field suggests that it is a sustainable, and perhaps under-utilized resource. Combined, Brady's and Desert Peak generate 18 MW net power, both from binary plants.

Both the Brady's and Desert Peak geothermal systems produce fluids with elevated total dissolved solids (TDS) and sodium levels, even compared to other systems in Nevada. Brady's wells have TDS levels generally between 2700 and 3300mg/L with sodium concentrations between 850 and 950mg/L. Desert Peak wells produce fluids with TDS between 8000 and 9000mg/L, with sodium levels on the order of 2700mg/L. In comparison, the Beowawe geothermal system near Battle Mountain, NV has TDS levels between 300 – 1000 TDS (Garg et al., 2007). This is an important distinction to make when interpreting resistivity surveys in these regions, as higher TDS values will be associated with decidedly lower formation resistivity's. This is especially true where high porosity units such as the Truckee River Formation are present.

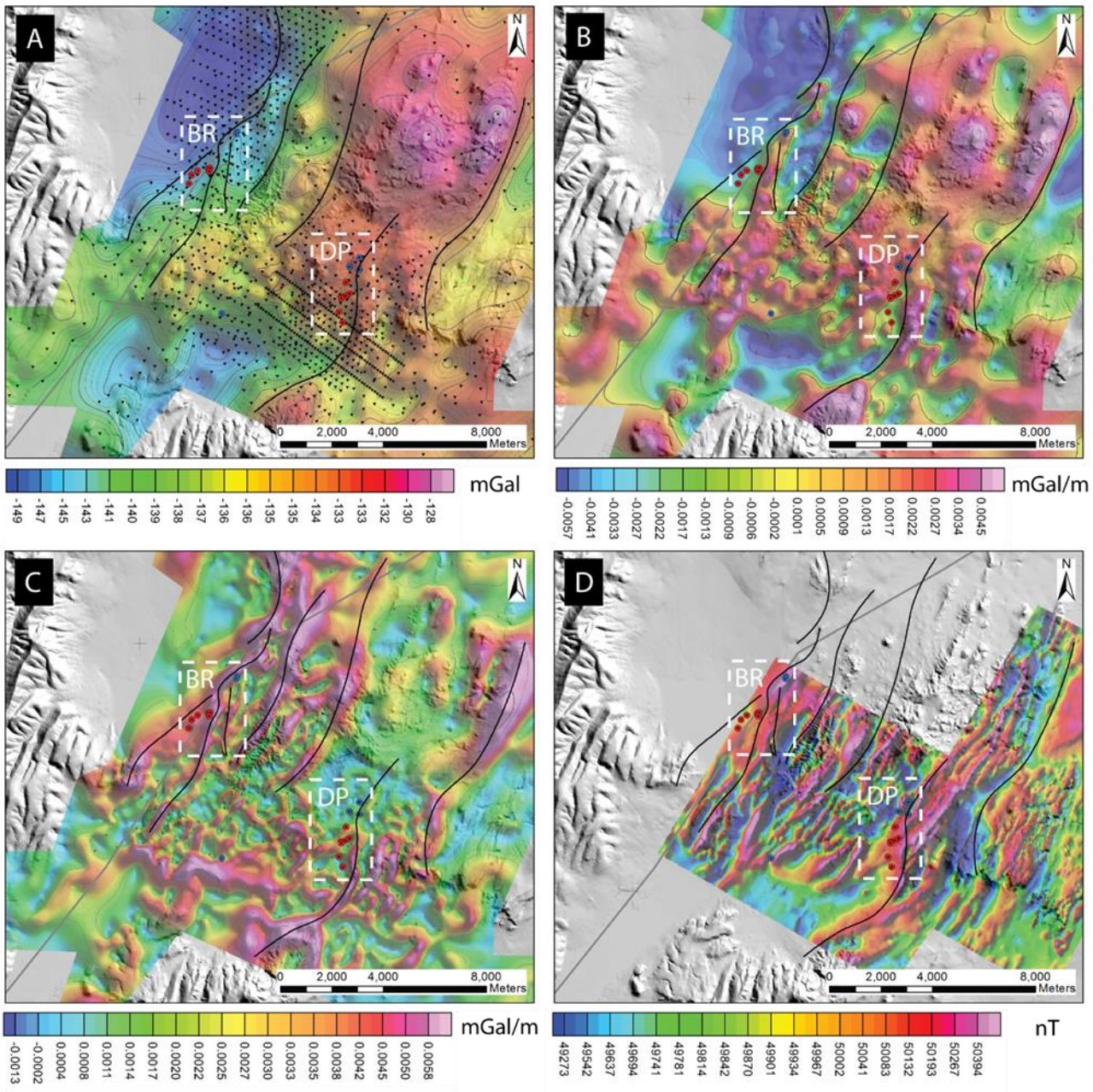


**Figure 2: Gravity and aeromagnetic data for the study area. BR, Brady's geothermal field; DP, Desert Peak geothermal field. A: Complete Bouguer anomaly map at a reduction density of 2.35g/cm$^3$. Black inverted triangles denote gravity stations. B: First vertical derivative of the Bouguer anomaly, upward continued 50m. The first vertical derivative highlights near-surface dense bodies. This map correlates well with near-surface, dense volcanic units such flow basalts and andesites. C: Horizontal gradient magnitude of the Bouguer anomaly. This map highlights areas where the gravity is changing quickest in any horizontal direction, and is useful for locating faults with a large density contrast on either side. D: Reduced-to-pole helicopter-magnetic survey. Survey flown with 200m line spacing and 30m terrain clearance.**

## 3. METHODS

This section discusses the methods for collecting, processing and modeling the gravity and CSAMT datasets presented in this paper.

### 3.1 Gravity

The gravity data presented in Figure 2 includes hundreds of previously unpublished stations collected by Zonge International. Three separate campaigns performed by Zonge in 2009, 2013 and 2017 were added to gravity data collected by Gary Oppliger in 2003 and 2004 (Presented in Faulds et al., 2010). The current data set has a total of 1673 stations and is gridded at 50m. Both Scintrex CG-5 and LaCoste

and Romberg Model-G gravimeters were employed. Elevation data was collected using survey-grade Leica Geosystem model VIVA GS15 GPS/GLONASS receivers. A single GPS base station (917006) was used for the survey. Two gravity base stations were employed, both locally established from three-loop traverses to gravity base "RENO" at the James G. Scrugham Engineering Mines Building at the University of Nevada, Reno.

Gravity data was processed to a complete Bouguer anomaly map using the Gravity and Terrain Correction software version 8.4 for Oasis Montaj. All elevations are referenced to the Geoid using the GEOID 12A model (NAVD88). Processing included the Bullard B correction to correct for the spherical nature of the upper crust (LaFehr 1991). Of the presented data, only the first vertical derivative has been upward continued to 50m (Figure 2 B). Reduction density of 2.35g/cm$^3$ was chosen to minimize correlation with topography and reflect upper-crust and near-surface density anomalies.

**3.2 CSAMT**

Unlike natural-source magnetotellurics (MT), CSAMT depends not on natural EM sources from the ionosphere, but rather from a grounded dipole transmitter located a few km from the survey lines. In natural source MT, EM waves are vertically incident upon the ground surface, where most of the energy (nearly 100%) is reflected by the conductive earth, but a tiny portion is transmitted (Jiracek et al., 1995). EM waves travel indefinitely in a vacuum, but in a conductive media (the Earth) the mode of transmission changes. The waves diffuse downward, and diminish exponentially with depth. This attenuation is affected by the frequency of the waves and the resistivity of the media; lower frequency energy penetrates further, and all waves penetrate more deeply in resistive media. This phenomenon is known as the skin depth, and can be thought of as a proxy for the depth of investigation. In CSAMT, the transmitter is a dipole set up parallel to survey lines. EM waves move along the surface of the earth and propagate nearly vertically into the ground. CSAMT benefits from higher signal-to-noise ratios, which enables rapid data collection. A disadvantage is that these EM waves penetrate vertically into the ground only for distances greater than half a wavelength. This is referred to as the 'far-field', and in that zone simplified MT equations describing apparent resistivity and phase are valid. At shorter distances, 'near-field' effects bias the data to be more resistive. In practice, this limits on how deep the CSAMT method can see. At distances far from the transmitter, the signal becomes small and less usable.

In the far-field, the apparent resistivity, $\rho_a$, is estimated by measuring variations in the orthogonal components of electric field, E and magnetic field, H at the surface. The coordinate system used is such that the survey line direction is the x-direction, with the y-direction perpendicular to this. The apparent resistivity is a function of frequency, first described by Cagniard (1953):

$$\rho_a(\omega) = \frac{1}{5f}\left|\frac{E_x(\omega)}{H_y(\omega)}\right|^2 \quad (1)$$

Where $\omega = 2\pi f$. The impedance phase is also measured and is simply the phase delay of the electric field with respect to the magnetic field. The impedance phase is an important part of the data and describes how resistivity changes with depth. In CSAMT the phase is straight forward to estimate because the transmitter and receiver are in communication with one another and the transmitted phase signal is known. Taken together, the apparent resistivity and phase represent the data upon which models are built.

Zonge International performed two CSAMT surveys over the study area. An early survey, conducted in 2003, completed two lines with 100m station spacing near Desert Peak (lines 11 and 12, Figure 3) A subsequent survey in 2017 added 10 survey lines in both the Brady's geothermal field and southwest of Desert Peak. Both surveys collected data between 1 – 8192Hz. Lines near Brady's were collected with 50m dipole spacing, and longer lines south of the field were collected with 100m dipole spacing. Gaps in the data exist where some lines crossed the interstate. Data was collected using Zonge GDP-3224 receivers. The survey was set up in a moving broad-side array, where data are collected in blocks consisting of four electric dipoles along the survey line and one magnetic antenna coil perpendicular to the line. Non-polarizable, porous pot, Cu-$CuSO_4$ electrodes were used to collect electric field data, and Zonge ANT/6 induction coil antennas were used to collect magnetic field data. Two transmitter locations were used for the 2017 survey. Power for the transmitter was produced from a motor-generator and transmitted via a Zonge GGT-30 transmitter. Communication between the transmitter and receiver was handled using a Zonge XMT-G GPS transmitter controller.

CSAMT data was modeled by Ormat staff using Geotools software by CGG. Raw station data was edited to remove near-field effects, stations with excessive static shift, and stations that were impacted by close proximity to power lines or other coherent noise sources. Each survey line was independently modeled using both 1D and 2D inversion routines. Smooth 1D models (12 layers per decade) were generated using estimated data errors and a noise floor of 5% for apparent resistivity and 2.5% for the impedance phase. A simple, 5ohm-m starting model was used that is representative of the background resistivity for this area. Once 1D models had been generated for all stations in the study area, the resistivity was contoured using a least squares grid fit at fixed elevations to show changes with depth in map view (Figure 3). A tension weight of 0.1 was employed which helps reinforce trends between lines in the gridding algorithm. However, this had minimal effect on the results.

This process was repeated using a 2D, non-linear conjugate gradient inversion algorithm, producing model transects along each line (Rodi and Mackie, 2001). CSAMT data was modeled using the transverse magnetic mode, and topography was included. The starting model for each line was a 5ohm-m half-space, discretized horizontally such that a minimum of 5 cells exist between station locations (e.g., 12.5m cell widths for 50m dipole surveys). In the vertical direction, cells including topography were discretized to 4m, and below topography the cells increase in size using uniform scaling factor of 1.06. Excessive padding is added to the edges of the domain to address boundary conditions. A suite of inversions was performed for each line to find a balance between data misfit and model roughness. Once these lines were complete, we extracted resistivity data at each station location and produced depth-slice maps similar to those made using 1D models. The difference between these maps using 1D and 2D results was found to be minimal, and so the 1D results are presented (Figure 3).

**4. RESULTS**

Interpretation of Figure 3 requires a basic understanding of the 1D inversion routine. 1D models presented here are generally sensitive to 150 – 500m deep, dependent on the vertically-integrated conductance in any region. In more resistive areas the depth of investigation is deeper. The models are also sensitive to the near-field effects inherent in CSAMT, which differs between stations and renders the lowest frequencies unusable in places. Finally, the deepest modeled value in any one sounding persists to infinite depth, despite the fact that the data is no longer sensitive to it. This means that if the deepest value in a 1D model is 5 ohm-m, then beneath that the model is also 5 ohm-m to infinite depth. In higher elevation locations such as near Desert Peak, the deepest depth slices look beneath the sensitive range and so the resistivity values stop changing.

Because the geothermal systems at Brady's and Desert Peak are at different elevations, the pertinent changes occur in different panels of Figure 3. For Desert Peak, the changes are best shown in Figure 3 A-F. The 1D models here cannot see below ~1200 m elevation near Desert Peak for the most part. The pertinent changes at Brady's are best seen in panels E-I of Figure 3. Blank areas in Figure 3 A-D are due to the low elevation of the topography there.

At Desert Peak, a small point of low resistivity (1-2ohm-m) along CSAMT line 12 is the shallowest conductive feature associated with smectite clay alteration. The presence of smectite clays was confirmed by X-ray diffraction in the upper portions of several Desert Peak wells (Lutz et al., 2009). This feature is immediately adjacent to the RRFZ and located near the northernmost production wells in the field (Figure 3 A). As depth increases, this dome-shaped conductor broadens, but its eastern edge is truncated by the RRFZ (Figure 3 B-C). As the models deepen, the area of low resistivity becomes larger, and moves down elevation and into the small sedimentary basin SW of the Desert Peak wells. Between 1275 and 1200m elevation, the low-resistivity anomaly fills the majority of this small basin and does not appear to merge with anomalies at Brady's. Although precise water-level maps are not available for this basin, we assume that elevation is good proxy for the water table. The low resistivity zone appears to move down the hydrologic gradient. The RRFZ continues to truncate the anomaly at least until it intersects line 9 (Figure 3 E), which suggests that it is an important hydrologic barrier. This observation is somewhat dependent on the end of line 8, which unfortunately stops right at the fault. It is possible that up-flow occurs along some length of the RRFZ, flowing westward into the basin and altering the sediments there. Close inspection does hint at additional up-flow zones, but none so striking as the main anomaly on line 12 (Figure 3 A-C). If we assume that all outflow originates from a point source near the anomaly in Figure 3A, it should not be able to flow 'uphill'. Yet in parts of this dataset that seems to occur, such as small zone on the western end of line 12 that begins at 1275m. Perhaps these areas host additional small up-flow zones.

At Brady's, the zone of low-resistivity alteration is mostly confined to the western flank of the BFZ. As depth increases, the zone moves basin-ward and broadens in width. Lines 3, 4 and 5 mark the edge of the anomaly to the NW, so the anomaly is not well constrained here. We theorize that had the survey continued NW it would show deeper and broader anomalies as the basin deepens. Although the surficial evidence of a geothermal system is about 4 km long on the BFZ, the resistivity suggests that alteration has occurred along ~8km of the fault zone. A prominent left step in the resistivity anomaly occurs at lines 6 and 7 (Figure 3 F-I), corroborating the observations of Faulds et al. (2006; 2010).

A surprising find is a prominent zone of alteration on the east side of the BFZ. This anomaly is best seen on line 4 in Figure 3 E-G. Updated gravity maps (Figure 2) suggest that the BFZ bounds a small horst to the west, and a graben exists between the BFZ and the range front to the east. The horst structure is also supported by a resistive zone in the centers of lines 4 and 5. The alteration here is relatively shallow and diminishes in size with depth; it is one of the few places where the CSAMT sees below a conductive feature. It is unclear if this eastern zone of alteration at Brady's is sourced from the BFZ, the range front fault immediately to the east, or by some other feature.

We constructed several 2D gravity forward models along WNW transects that cross the dataset. One of these models, parallel to CSAMT line 4, is presented in Figure 4 A-C. This azimuth is perpendicular to both the strike of regional fault blocks and to major gravity contours, which help make the assumptions inherent in 2D modeling valid. To constrain the non-uniqueness of these models, drill data, Lidar, geologic maps (Faulds and Garside, 2003), and geologic cross sections from literature were considered.

A detailed study of formation densities and porosities was performed prior to modeling the gravity data. The densities used to build the model are summarized in Figure 4 B. Density estimates for the Mesozoic basement, Rhyolite and Chloropagus Formations come from drill core analyzed by Lutz et al. (2004). Ormat performed a detailed study of densities within the Truckee River Formation, which were found to be highly variable. This formation is composed of fresh water limestone, diatomite, tuffaceous siltstones and various thin layers of basalt. Samples were recovered both from the surface and from shallow drill core at wells BCH-7, BCH-8 and BCH-10. Laboratory testing estimated both dry bulk density using Archimedes principle, and grain density via helium pycnometer. Having both densities allows for estimation of the porosity, and estimation of sample density if it were 100% saturated. Of five samples of basalt found in the Truckee River Formation, we estimated a mean saturated density of 2.50 g/cm$^3$ and porosity of 0.13. From nine fresh water limestone samples, we estimated a mean saturated density of 2.37g/cm$^3$ and porosity of 0.23. From 8 samples of tuffaceous sediments (all from drill core at BCH wells) we estimated a mean saturated density of 2.43g/cm$^3$ and porosity of 0.19. From 7 samples of diatomite we estimated a mean saturated density of 1.69 g/cm$^3$ and porosity of 0.54. Estimates of the diatomite may not be well constrained, as several samples floated on water during testing. Diatomite is prevalent in the shallow surface of the study area, and is mined commercially 5km NW of the Brady's plant.

The presence of the diatomite complicates gravity modeling efforts due to its close proximity to the surface and exceptionally low density. We assigned a generic value of 2.2 g/cm$^3$ to the Truckee River Formation, but in places with high concentrations of diatomite this could be off by 0.5 – 0.6 g/cm$^3$. In areas where clear evidence of diatomite exists, we locally reduced the density of this formation to as far as

2.0 g/cm$^3$. Depth estimates to Truckee River contacts may be off by as much as 30%, and in areas replete with diatomite, the depths are likely overestimated.

The 2D forward model shown in Figure 4 B illustrates the requirement for a low-density body, or down-thrown block just east of the BFZ. Unfortunately, no drill records are available east of the BFZ and into this downthrown block or the east-dipping fault that bounds it. A thorough review of drilling records in Brady's field reveals that no well has pierced this zone. The closest to it, well 68A-1, appears to have drilled directly into the top of the horst. This well encountered no lost circulation zones, no sedimentary rocks of the Truckee River Formation, and hit both the younger volcanic sequences and the Rhyolite Formation at shallower depths than surrounding wells. The dotted box in Figure 4 C represents the location of a 2D inversion of CSAMT data (shown in Figure 4 D). This CSAMT line passes through the low-resistivity feature east of the BFZ and also supports the presence of a horst-like structure. Taken together, these models suggest that smectite-clay alteration occurs more readily in Quaternary fill and Truckee River Formation strata.

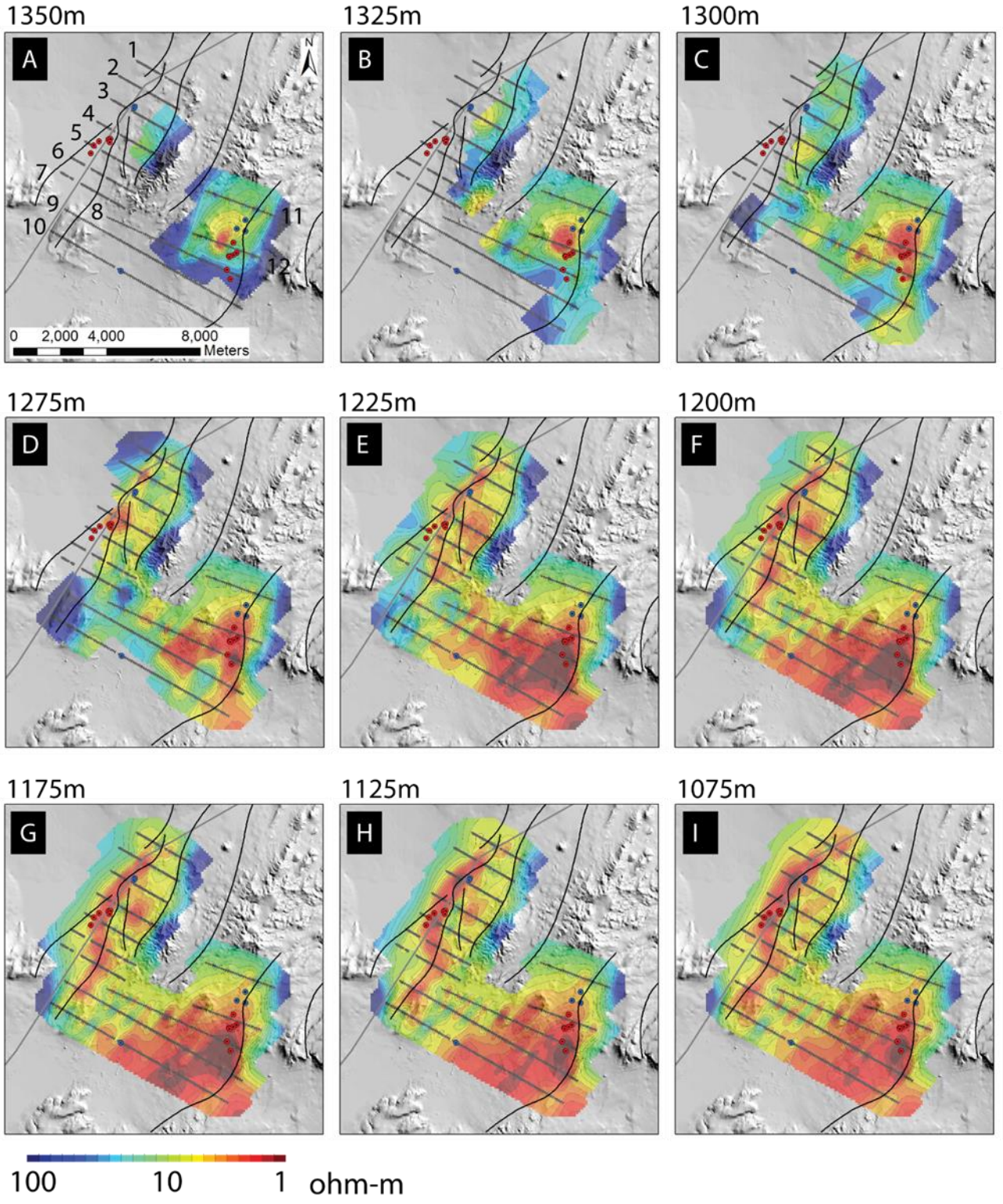


**Figure 3: Contoured depth-slices through 1D CSAMT resistivity models at key elevations. Station locations are shown as small inverted black triangles, though they overlap at this scale. Production wells are shown as red dots; injection wells are shown as blue dots. Inferred faults are shown as black lines. Brady's wells east of I-80 produce from 700 – 900m elevation, and wells west of I-80 produce from -490 – 390m elevation. Desert Peak wells produce from 1115 – 135m elevation.**

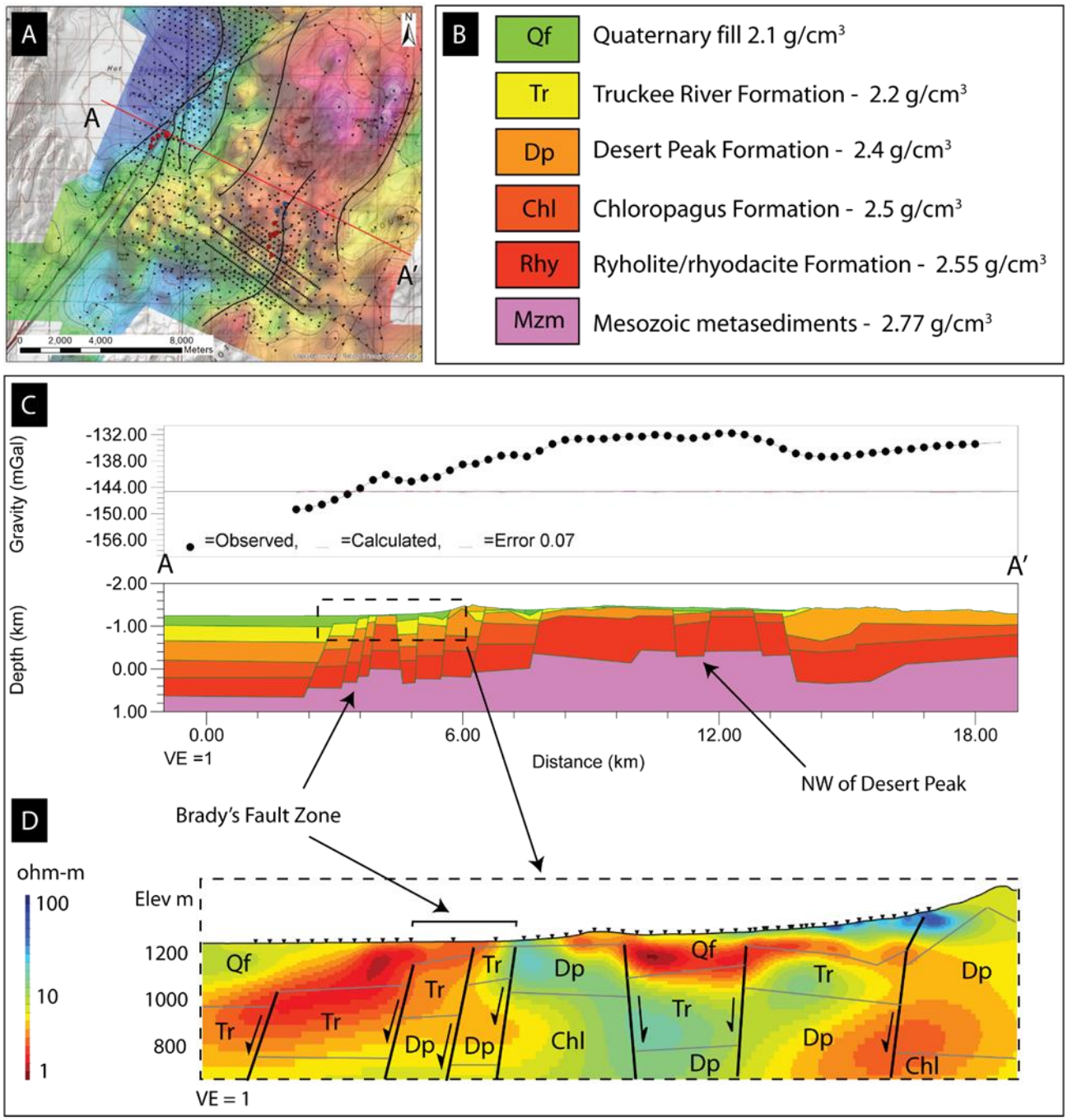


**Figure 4: A: Complete Bouguer anomaly map with model transect AA' in red. Geothermal production wells are shown as red dots and injection wells as blue dots. Inferred faults from gravity are shown as black lines. B: Estimated bulk densities for various Formations. C: 2D gravity forward model, with model response and data fit above. The dashed box shows the domain for a parallel 2D CSAMT inversion. D: 2D inverse model of CSAMT data along line 4 (see Figure 3).**

## 5. DISCUSSION

Shallow imaged resistivity, mapped at high resolution, clearly shows a low-resistivity anomaly moving down-gradient in the small basin SW of the Desert Peak geothermal system. However, it is difficult to say how much of this anomaly is due to smectite-clay alteration, and how much is due to the high TDS levels present in Desert Peak geothermal fluids. Near to the high-elevation points of the anomaly, wells frequently encounter sequences of smectite clay alteration at the depths imaged by CSAMT. At distances further away, but still within the low-resistivity anomaly it is less clear if this is the case. A recent chemistry analysis collected during a flow test of geothermal production well 74-28 indicated TDS concentrations of 8900mg/L, with sodium and chloride together amounting to 7800mg/L. The fluid measured a resistivity of 1.2ohm-m at 20°C. Were this fluid to saturate a hypothetically 'clean' sandstone with porosity of 0.25, a quick

estimate using Archie's Law (Archie, 1952) suggests the formation resistivity would be in the range of 12 – 32ohm-m. However, the resistivity of brines follows an inverse exponential dependence to temperature (Ussher, 2000). Based on the experiments of Ucok et al. (1980), the same fluid at 100°C would have a resistivity on the order of 0.3ohm-m. Formation resistivity's of the same clean sandstone at this temperature could be 3 – 8ohm-m. These estimates would decrease with increasing porosity, and our laboratory experiments have shown diatomaceous sediments in the study area with porosities approaching 0.5. It is not difficult to imagine that some combination of elevated-temperature and high TDS fluid in the right rock type could achieve the values imaged in this survey with minimal clay alteration. At Brady's, the salinity of outflow is significantly lower and so the distinction between smectite-clay alteration and unaltered, saturated porous rocks should be more clear.

Interestingly, a commercial salt-works operated between 1870 - 1915 where the small basin SW of Desert Peak spills west toward I-80 (Figure 1). The history of this operation is discussed by Benoit (1982). The salt was produced by evaporating brines in vats that were dug into the ground, and are still visible in satellite imagery. Originally the brines emanated from springs, but later on they were pumped from shallow depths. Given the salinity levels of Desert Peak outflow, it begs the question of whether or not the geothermal system is the source of brine. Gravity data shows a subtle rise, or horst, precisely where this small basin opens to the west (Figures 1 and 2A). Assuming this represents a shallowing of denser and lower-permeability rock units, this geometry could force brines in the deeper portion of the basin to rise here. Upwelling of deep brines over buried horsts has been well-documented along the Rio Grande (Phillips et al., 2003; Hogan et al., 2007). The relict salt operation is located precisely at this point.

## 6. CONCLUSIONS

High-resolution CSAMT data can successfully map geothermal out-flow patterns of Basin and Range style geothermal systems. These outflow patterns can be complex, but generally flow down-gradient towards basins or other drainages. Since resistivity is sensitive to hydrologic parameters such as ion concentration, temperature and porosity, it can reveal the source and patterns of fluid migration that other geologic and geophysical techniques cannot. When used in concert with other methods, this type of data set can better inform workers on which faults are the most productive, at least in the upper ~300m. As an exploration strategy, finding the highest elevation point of a smectite-clay alteration feature is promising; at Desert Peak, had the CSAMT data set been the only available information, it would have pointed directly to the resource (Figure 3 A-C). However, the likelihood that this strategy can be successful seems to depend on the presence of high-porosity strata that can easily be altered to clay. Further complicating the strategy's efficacy is the nature of the geothermal outflow fluids; warm high-salinity fluids can mimic smectite-clay alteration in the resistivity results. Although we cannot say with confidence where smectite-clay alteration ends along such flow paths, it is likely that the Desert Peak System has been discharging fluids into the adjacent basin for a long time.

At Brady's, the method has highlighted a curious target east of the BFZ that, along with gravity data, suggests an east-dipping fault and small horst and graben structure. This target may be a source of additional production or have adequate transmissivity for injection; either finding would benefit the field. The results also agree with previous workers that a prominent left-step in the BFZ may be contribute to high transmissivity there. Finally, the CSAMT results suggest that, at least in the near surface, the Brady's and Desert Peak systems are not connected.

## REFERENCES

Archie, Gustave Erdman. Classification of carbonate reservoir rocks and petrophysical considerations. *AAPG Bulletin* 36.2 (1952): 278-298.

Benoit, D. Forced folding and Basin and Range geothermal systems. No. CONF-951037. *Geothermal Resources Council, Davis, CA* (United States), 1995.

Benoit, Walter R., John E. Hiner, and Robert T. Forest. *Discovery and geology of the Desert Peak geothermal field: a case history. Bulletin 97*. No. NP-4900578. Nevada Univ., Reno (USA), 1982.

Cagniard, Louis. Basic theory of the magneto-telluric method of geophysical prospecting. *Geophysics* 18.3 (1953): 605-635.

Cumming, William, and Randall Mackie. Resistivity imaging of geothermal resources using 1D, 2D and 3D MT inversion and TDEM static shift correction illustrated by a Glass Mountain case history. *Proceedings World Geothermal Congress 2010*. 2010.

Cumming, William. Geothermal resource conceptual models using surface exploration data. *Proceedings, Thirty-Fourth Workshop on Geothermal Reservoir Engineering*. 2009.

Faulds, James E., et al. Structural controls of geothermal activity in the northern Hot Springs Mountains, western Nevada: The tale of three geothermal systems (Brady's, Desert Peak, and Desert Queen). *Geothermal Resources Council Transactions* 34 (2010): 675-683.

Faulds, James E., et al. Characterizing structural controls of geothermal fields in the northwestern Great Basin: A progress report. *Geothermal Resources Council Transactions* 30 (2006): 69-76.

Faulds, James E., Larry J. Garside, and Gary L. Oppliger. Structural analysis of the Desert Peak-Brady geothermal field, Northwestern Nevada: implications for understanding linkages between Northeast-trending structures and geothermal reservoirs in the Humboldt structural zone. *Transactions-Geothermal Resources Council* (2003): 859-864.

Faulds, James E., Larry J. Garside, and Robert Chaney. Preliminary geologic map of the Desert Peak-Brady geothermal fields, Churchill County, Nevada. *Nevada Bureau of Mines and Geology*, 2003.

Garg, Sabodh K., et al. Characterization of geothermal reservoirs with electrical surveys: Beowawe geothermal field. *Geothermics* 36.6 (2007): 487-517.

Hogan, James F., et al. Geologic origins of salinization in a semi-arid river: The role of sedimentary basin brines. *Geology* 35.12 (2007): 1063-1066.

Hulen, Jeffrey B., and Susan J. Lutz. Altered volcanic rocks as hydrologic seals on the geothermal system of Medicine Lake volcano, California. *Geothermal Resources Council Bulletin* 28.7 (1999): 217-222.

Jiracek, G. R., V. Haak, and K. H. Olsen. Practical magnetotellurics in a continental rift environment. *Developments in Geotectonics* 25 (2006): 103-129.

Rodi, William, and Randall L. Mackie. Nonlinear conjugate gradients algorithm for 2-D magnetotelluric inversion. *Geophysics* 66.1 (2001): 174-187.

LaFehr, T. R. Standardization in gravity reduction. *Geophysics* 56.8 (1991): 1170-1178.

Lutz, S., et al. Geological and structural relationships in the Desert Peak Geothermal System, Nevada: Implications for EGS development. *Proceedings 34th Workshop on Geothermal Reservoir Engineering*. 2009.

Lutz, Susan Juch, et al. Lithologies, hydrothermal alteration, and rock mechanical properties in wells 15-12 and BCH-3 Bradys Hot Springs geothermal field, Nevada. *GRC Transactions* 35 (2011): 469-476.

Phillips, Fred M., et al. Environmental tracers applied to quantifying causes of salinity in arid-region rivers: results from the Rio Grande Basin, Southwestern USA. *Developments in water science* 50 (2003): 327-334.

Ucok, Hikmet, Iraj Ershaghi, and Gary R. Olhoeft. Electrical resistivity of geothermal brines. *Journal of Petroleum Technology* 32.04 (1980): 717-727.

Ussher, Greg, et al. Understanding the resistivities observed in geothermal systems. *Proceedings world geothermal congress*. 2000.